Available online at www.sciencedirect.com
ScienceDirect
Ceramics International 36 (2010) 1511–1516
CERAMICS INTERNATIONAL
www.elsevier.com/locate/ceramint

Densification and grain growth of CuO-doped Pr_6O_{11} varistors

T.Y. Li *, H.Q. Wang, Z.Q. Hua, L. Dong, H.W. Zhao, Y. Wang

Key Laboratory of Advanced Technologies of Materials (Ministry of Education of China), Superconductivity R&D Center (SRDC), Mail Stop 165#, Southwest Jiaotong University, Chengdu, Sichuan 610031, People's Republic of China

Received 24 August 2009; received in revised form 22 December 2009; accepted 2 February 2010
Available online 9 March 2010

Abstract

The effect of CuO doping on the microstructure and electrical properties of Pr_6O_{11} varistors was investigated. Samples were prepared by conventional ceramic techniques, and were sintered at 1150 °C in air for 2 h. The microstructure was investigated by scanning electron microscopy (SEM). The phases and chemical composition were analyzed by X-ray diffraction (XRD) and energy dispersive spectroscopy (EDS). The results indicated that CuO can promote the densification of the Pr_6O_{11}-based varistors to 95.8% of the theoretical density. CuO forms a solid solution with Pr_6O_{11} up to 0.5 mol%, above which Pr_2CuO_4 precipitates in the grain boundary. From the *I–V* measurements, minor CuO doping can improve the nonlinear electrical properties. A further increase in CuO content induces a reduction in the nonlinear electrical properties due to the consumption of absorbed oxygen on the grain surfaces.

Keywords: E. Varistors; Densification; Pr_6O_{11}; CuO

1. Introduction

Varistors are electronic ceramic devices that show nonlinear electrical properties. They are widely used to protect electrical and electronic equipment against transient overvoltages. Today, the majority of varistors produced commercially are based on ZnO with minor additions of typically Bi_2O_3, Sb_2O_3, CoO, MnO_2 and Cr_2O_3 [1–3]. Other varistor systems based on SnO_2 [3], $SrTiO_3$ [4], TiO_2 [5], WO_3 [6], $CaCu_3Ti_4O_{12}$ [7] and Tb_4O_7 [8] have been reported in the literature. The non-ohmic behavior is now known to be due to the existence of double Schottky barriers at the grain boundaries, created during sintering process. However, many aspect related to these materials remain unclear [9–11], such as conduction mechanism of the double Schottky barriers and physical origin of the interface states. In addition, commercial varistors based on ZnO present a high nonlinear coefficient, but the degradation problem has not been resolved [12–14].

Recently, a new varistor system based on Pr_6O_{11} was first introduced by our research group and nonlinear electrical properties were observed. The simple microstructure, consisting generally of one phase under X-ray resolution, is the main characteristic of this ceramic [15]. This novel varistor system is helpful not only in further understanding of the problems that still remain unclear but also in satisfying the need for better electrical properties. However, the use of praseodymium oxide varistors is limited by the low densification during sintering process. The bonding energy of surface oxygen to praseodymium is weak due to the low symmetry structure, the oxygen ions can readily escape from the original sites when the temperature exceeds 400 °C [16]. Cu_2O has a high symmetry structure with strong bonding energy. There is a possibility that Cu can substitute for Pr ions in the lattice and thereby improving the densification process. CuO was used as the starting material because of CuO can be transformed into Cu_2O when the temperature is higher than 1000 °C [17]. The purpose of the present work is to investigate the influence of CuO on the microstructure and electrical properties of Pr_6O_{11}-based varistors.

2. Experimental procedure

The raw materials used in this work were analytical grades of Pr_6O_{11} (99%, Yuelong Inc., China) and CuO (99%, Kemiou Inc., China). Samples with nominal compositions $(100 - x)$

* Corresponding author. Tel.: +86 02887601824; fax: +86 02887600787.
E-mail address: tongyeli@yahoo.cn (T.Y. Li).

0272-8842/$36.00
doi:10.1016/j.ceramint.2010.02.028

$PrO_{1.83} + x$ CuO, where $x = 0.0$, 0.1, 0.5, 1.0, 5.0 and 10.0 mol%, were produced using a conventional mixed oxide processing route. After milling in an agate mortar for 3 h, calcining was performed at a constant heating rate of 100 °C/h up to 800 °C in air. The calcined mixture was pulverized using an agate mortar and after 2 wt% polyvinyl alcohol (PVA) binder addition, the aqueous slurry was then dried using an oven at 80 °C to obtain the granulated powders. The powders were pressed at 100 MPa to form discs 10 mm in diameter and 1.0–1.5 mm in thickness. The discs with same concentration were sintered at 1150 °C in air for 2 h. The heating rate was maintained at 100 °C/h. A pycnometer (ACCUPYC 1330) was used for density measurements. The sintered samples were crushed and placed in a receptacle to determine the phase constitutions by X-ray diffraction technologies (7602EA ALMELO) under the following experimental condition: 40 kV, 40 mA, $20^\circ \leq 2\theta \leq 90^\circ$, $\lambda(\mathrm{Cu}K_\alpha) = 0.15406$ nm, $\Delta 2\theta = 0.0167^\circ$, step time = 10.160 s. The lattice parameters were calculated from the X-ray diffraction patterns using a least squares fit. The microstructure of fractured samples was examined using scanning electron microscopy (FEI QUANTA200 with an energy dispersive spectrometer). As for the SEM analysis, samples were cleaned in acetone, mounted, and gold-coated to prevent charging. Grain sizes were determined by the linear intercept method. Chemical analysis was performed using auger electron spectroscopy (AES, PHI 700). For electrical measuring, In–Ga mixed alloy (the purity of both are 99.999%, In:Ga = 1:1) as electrode material was painted on both polished surfaces of samples. The electrode area was about 0.64 cm^2. The impedance measurements were made with a frequency response analyzer (HP4294A) using frequency ranging from 40 Hz up to 13 MHz, with an amplitude voltage of 0.5 V. The current-voltage (I–V) characteristics of the sample were measured using a DC electric source (Keithley 2400 with the precision of 0.035%).

3. Results and discussion

The XRD patterns for all six compositions of Pr_6O_{11}-based varistors are given in Fig. 1. It is evident that the main phase of all the samples is Pr_6O_{11} (JCPDS file card number 042-1121), which has a fluorite structure. Samples containing less than 5.0 mol% CuO do not exhibit the presence of any additional peaks corresponding to the secondary phases which are formed during the sintering process. The secondary phase is identified as Pr_2CuO_4 with the tetragonal structure (JCPDS file card number 049-1891) through an XRD analysis. The calculated lattice parameters, as listed in Table 1, decrease with increasing CuO content, which imply the formation of solid solution.

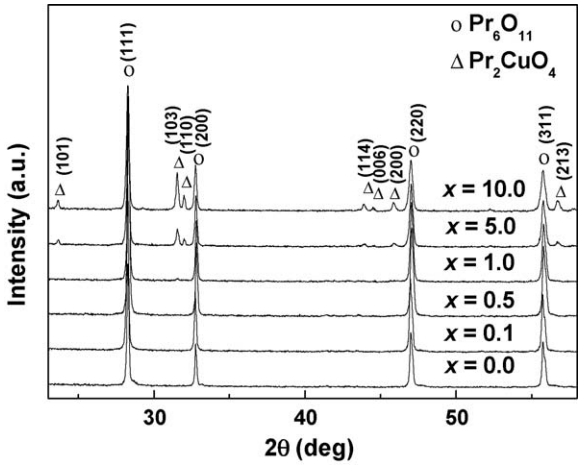

Fig. 1. X-ray diffraction patterns of the ceramic samples.

Fig. 2 shows the typical scanning electron micrographs of the ceramic samples. The SEM images elucidate the changes in the grain structure with increasing CuO content. The values of the relative density were calculated taking into account the chemical composition before sintering [18] and listed in Table 2. It can be seen that the samples with small amounts of CuO are porous and have relatively small grains. The porosity of the ceramics reduces sharply with increasing CuO content. Doped CuO can facilitate the grain growth, as listed in Table 2. The EDS analysis indicates that Cu-rich phase is only found at the grain boundary regions when doped with 10.0 mol% CuO content, as shown in Fig. 3.

The electrical properties of the samples, characterized by its current–voltage characteristics, are shown in Fig. 4. It is seen that the entire I–V curve is shifted to the left with increasing CuO content. In order to compare with conventional varistor system, the nonlinear coefficient (α) was obtained by the following equation:

$$\alpha = \frac{\log(I_2/I_1)}{\log(V_2/V_1)} \quad (1)$$

where V_1 is the voltage corresponding to I_1 = 1 mA/cm^2, and V_2 to I_2 = 10 mA/cm^2, respectively. The breakdown voltage (E_b) is the field density when the current density reaches 1 mA/cm^2. The leakage current density (J_L) was measured at 0.80 E_b. The calculated parameters are listed in Table 2. The nonlinear coefficient reaches a maximum ($\alpha = 1.7$) at 0.5 mol% CuO doping and then reduces with a further increase in CuO content. The sample presents linear I–V characteristics when doped with 10.0 mol% CuO. The breakdown voltage decreases with increasing CuO content, while the leakage current has no obvious change. Compared to the conventional varistor, the nonlinear coefficient is quite low. This is because the current interval used to calculate the nonlinear coefficient is located in the linear region of the current–voltage curves. For Pr_6O_{11} varistor, the current increases sharply when it exceeds 10 mA/cm^2, so the nonlinear coefficient was also calculated in

Table 1
Lattice parameters (a) and unit cell volume (V) of the sintered samples.

CuO (mol%)	a (Å)	$V = a^3$ (Å^3)
0.0	5.4601	162.7818
0.1	5.4570	162.5031
0.5	5.4537	162.2092
1.0	5.4473	161.6381
5.0	5.4441	161.3607
10.0	5.4408	161.0683

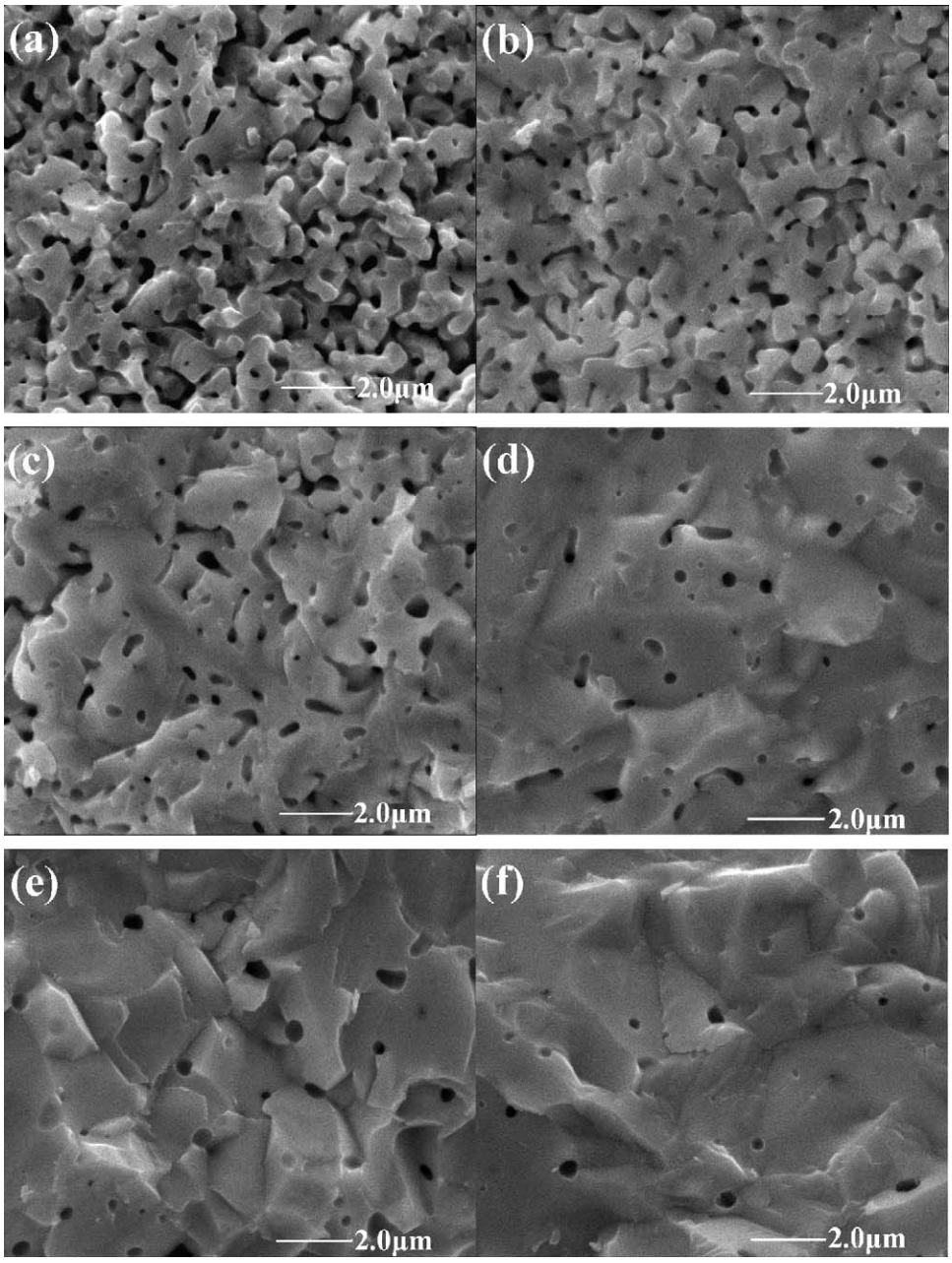

Fig. 2. Typical SEM micrographs of the samples prepared with different amounts of CuO: (a) $x = 0.0$; (b) $x = 0.1$; (c) $x = 0.5$; (d) $x = 1.0$; (e) $x = 5.0$; (f) $x = 10.0$.

Table 2
Some parameters of the samples with different CuO contents.

CuO (mol%)	α	E_b (V mm^{-1})	J_L (mA cm^{-2})	Φ_B (eV)	d (μm)	ρ (%)[a]
0.0	1.4	25.2	0.77	0.11	0.6 ± 0.1	76.1
0.1	1.6	22.8	0.79	0.13	0.8 ± 0.1	80.3
0.5	1.7	19.6	0.77	0.18	1.2 ± 0.2	86.7
1.0	1.5	18.6	0.79	0.15	3.2 ± 0.4	92.2
5.0	1.2	6.3	0.79	0.08	3.3 ± 0.5	95.6
10.0	1.0	0.5	0.80	0.03	3.6 ± 0.5	95.8

[a] Theoretical density of Pr_6O_{11} is 6.88×10^3 kg/m^3. Theoretical density of CuO is 6.40×10^3 kg/m^3.

the current interval of 10–100 mA/cm^2, which can reach up to 18 when doped with 0.5 mol% CuO. However, the high leakage current is adverse for the application of Pr_6O_{11} varistor, so a further effort to reduce the leakage current is needed. As listed in Table 2, the values of potential barrier height, determined by I–V curves for different temperatures [19], have the same change trend as the nonlinear coefficient. Parallel straight lines were observed for the electric field and temperature range studied. The conduction mechanism for low electrical field is associated with thermionic emission of the Schottky barriers.

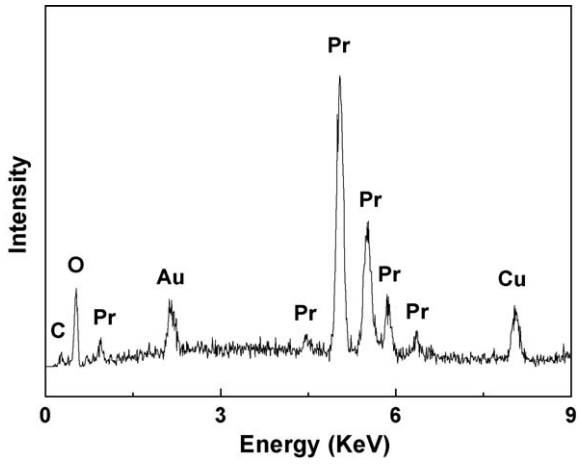

Fig. 3. EDS spectra of the grain boundary in the sample with 10.0 mol% CuO.

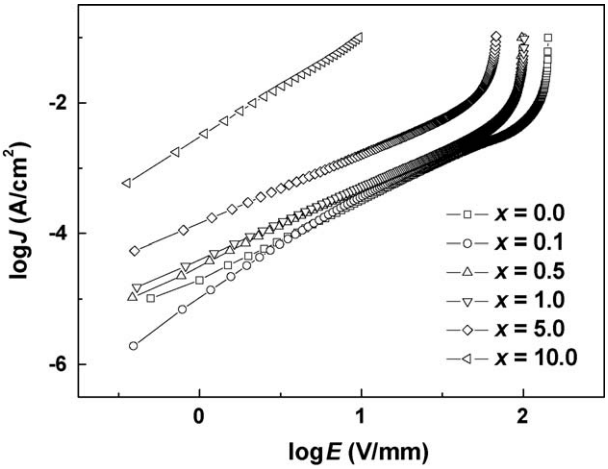

Fig. 4. Effect of Cu doping on the current–voltage characteristics of the Pr_6O_{11} varistors sintered at 1150 °C for 2 h.

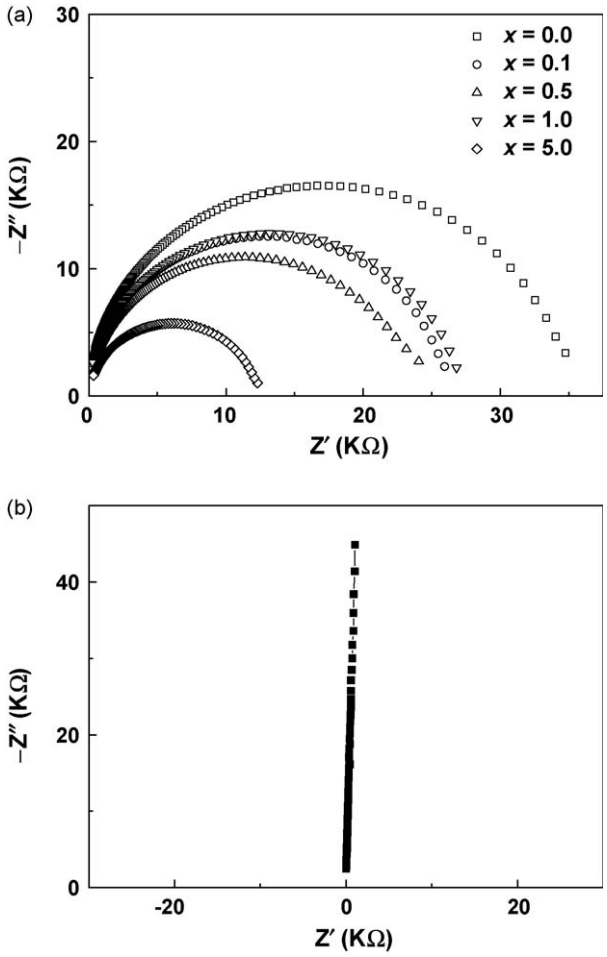

Fig. 5. Ac impedance spectra of the samples with different amounts of CuO: (a) $x = 0.0, 0.1, 0.5, 1.0, 5.0$. (b) $x = 10.0$.

Varistors consist of bulk and grain boundary regions, the impedance can be considered as two series-connected parallel *RC* (where *R* is a resistance and *C* is a capacitance) circuits due to the resistance and capacitance [20]. Since the grain resistance is too small compared with grain boundary contribution, the impedance diagram of $-Z''$ (negative reactance) versus Z' (resistance) of a varistor usually takes a form of a semicircle. Fig. 5 shows the typical ac impedance spectra for all six compositions of Pr_6O_{11} ceramics. A grain boundary semicircle is observed in the impedance spectra of the samples containing less than 10.0 mol% CuO, and doped CuO can reduce the grain boundary resistance of the samples. The impedance spectra of the sample doped with 10.0 mol% CuO is devoid of any grain boundary semicircle, grain boundary resistance almost disappears and the grain boundary capacitance is the only contribution to the frequency response [21]. Grain resistance is also an important parameter of varistors, however, a few works have been published in which suitable measurements directly yield grain resistance [22], so the influence of CuO doping on the grain resistance was not discussed in this paper.

Praseodymium oxide (PrO_{2-x}) is a nonstoichiometric *n*-type semiconductor with fluorite structure. This material has different oxygen compositions with x ranging from 0.0 to 0.5 due to the multiple oxidation states (+3 and +4) of Pr. The condition of commercial powder of praseodymium oxide is Pr_6O_{11} ($x = 0.17$), which is considered to be the compound of Pr_2O_3 and PrO_2 [23]. Similar to Tb_4O_7 varistors, Pr_6O_{11} also has oxygen storage capacity, the origin of the varistor action can be attributed to the existence of double Schottky barriers at the grain boundaries and the barrier height depends on the concentration of the oxygen adsorbed on the grain surfaces [8]. Fig. 6 shows the AES depth profile of oxygen obtained on the fracture surface of pure Pr_6O_{11} ceramic, an accumulation of oxygen at the interfaces is evident.

The ionic radius of Cu^+ (CN = 4), Pr^{3+} (CN = 6) and Pr^{4+} (CN = 6) is 0.060 nm, 0.099 nm and 0.085 nm, respectively [24]. The lattice parameters decrease with increasing CuO content means that CuO can form substitution solid solution with Pr_6O_{11}. The chemical-defect reaction using Kroger–Vink notation can be written as following equation:

$$3Cu_2O \longrightarrow xCu''_{Pr} + (2-x)Cu'''_{Pr} + \frac{6-x}{2}V_O^{\bullet\bullet} + Pr_6O_{11}, \quad x = 0 \text{ to } 2, \tag{2}$$

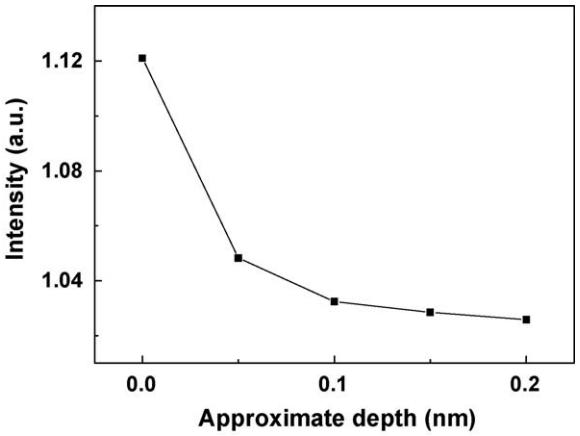

Fig. 6. The AES depth profile of oxygen obtained on the fracture surface of pure Pr_6O_{11} ceramic.

The displaced Pr ions can readily migrate to the grain boundaries and combine with oxygen at the fabrication temperature. The grain growth is enhanced by forming new Pr_6O_{11} lattice sites. Oxygen vacancies created by CuO doping will facilitate the grain boundary diffusion and bulk diffusion from the grain boundary area to the neck area, leading to the densification of the ceramic samples. When doped CuO exceeds the solubility limit, excess Cu segregates to the grain boundary to form the secondary phase. A further decrease in lattice parameters is observed with increasing CuO content, so there is the possibility that the segregated Cu can increase the substitution solid solution in grain interior. As a result, the densification and grain growth were further improved. The reason for the poor sintering of pure Pr_6O_{11} ceramics has not been reported, the high melting point should be the secondary factor. This is because pure Pr_6O_{11} ceramics have been sintered at higher temperatures and a significant increase in ceramic density was not observed. We suggest that the high vapor pressure due to the oxygen storage capacity is the main factor of the poor sintering.

Oxygen vacancies created by CuO doping will facilitate the oxygen adsorption by offering more oxygen adsorption sites, and thereby increasing the barrier height. With further increase in doping concentration, excess Cu_2O will be transformed into CuO by incorporating oxygen from the adjacent grain surfaces during the cooling process, followed by chemical interaction with Pr_2O_3 leading to the presence of Pr_2CuO_4 phase according to the following equation:

$$Cu_2O + \frac{1}{2}O_2 + 2Pr_2O_3 \rightarrow 2Pr_2CuO_4 \quad (3)$$

The adsorbed oxygen, which plays a key role in the formation of grain boundary barrier, disappears on the grain surfaces. The corresponding barrier height is also reduced. The total breakdown voltage along the single thread direction of the current flow is the product of breakdown voltage of each grain boundary and the number of grain boundaries. Grain growth can reduce the breakdown voltage by reducing the number of grain boundaries. Barrier height is directly proportional to the breakdown voltage of each grain boundary. Initially, the breakdown voltage slowly reduces with increasing CuO content. This is because the reduction of breakdown voltage can be delayed by the increase of barrier height. The breakdown voltage begins to reduce sharply when the barrier height reduces. The resistance of the samples under low electrical field, which is mainly provided by the grain boundary resistance, is proportional to the breakdown voltage [1,2], so it is proposed that the change of the grain boundary resistance is also controlled by the common effects of grain sizes and barrier height. The nonlinear coefficient reaches a maximum at 0.5 mol% CuO doping and then reduces when doped with 1.0 mol% CuO. This means that the secondary phase may be present at the grain boundaries when doped with 1.0 mol% CuO. However, the secondary phase was not found in the sample, which can be attributed to the detection limit of the X-ray diffraction.

4. Conclusions

In conclusion, CuO doping has a great effect on the microstructure and electrical properties of Pr_6O_{11}-based varistors. Oxygen vacancies created by CuO doping can facilitate the diffusion process, leading to densification and grain growth. Minor CuO doping can improve the nonlinear electrical properties by offering more oxygen adsorption sites. Samples with higher CuO content displayed the presence of a Pr_2CuO_4 phase precipitated at the grain boundaries, and the nonlinear electrical properties reduce sharply due to the consumption of the absorbed oxygen on grain surfaces in the formation of Pr_2CuO_4 phase.

Acknowledgment

This work was supported by the National Natural Science Foundation of China under Grant No. 50772092.

References

[1] T.K. Gupta, Application of zinc oxide varistors, J. Am. Ceram. Soc. 73 (7) (1990) 1817–1840.
[2] D.R. Clarke, Varistor ceramics, J. Am. Ceram. Soc. 82 (3) (1999) 485–502.
[3] P.R. Bueno, J.A. Varela, E. Longo, SnO_2, ZnO and related polycrystalline compound semiconductors: an overview and review on the voltage-dependent resistance (non-ohmic) feature, J. Eur. Ceram. Soc. 28 (3) (2008) 505–529.
[4] H.M. Ji, X.C. Liu, Y. Lv, C.X. Li, X.D. Chen, $SrTiO_3$ based dual-functional ceramics with nano-additives, Key Eng. Mater. 336–338 (2007) 793–795.
[5] A.B. Gaikwad, S.C. Navale, V. Ravi, TiO_2 ceramic varistor modified with tantalum and barium, Mater. Sci. Eng. B 123 (1) (2005) 50–52.
[6] X.S. Yang, Y. Wang, Y. Zhao, Effect of Dy_2O_3 and La_2O_3 on the microstructure and electrical properties of WO_3 ceramics, Mater. Chem. Phys. 98 (2–3) (2006) 225–230.
[7] S.Y. Chung, I.D. Kim, S.J.L. Kang, Strong nonlinear current–voltage behaviour in perovskite-derivative calcium copper titanate, Nat. Mater. 3 (11) (2004) 774–778.
[8] T.Y. Li, H.W. Zhao, L. Dong, N. Guo, Y. Wang, Novel varistor material based on terbium oxide, J. Phys. D: Appl. Phys. 42 (2009) 035401.1–035401.4.

[9] D.C. Look, Recent advances in ZnO materials and devices, Mater. Sci. Eng. B 80 (1–3) (2001) 383–387.
[10] M. Elfwing, E. Olsson, Electron holography study of active interfaces in zinc oxide varistor materials, J. Appl. Phys. 92 (9) (2002) 5272–5280.
[11] S. Hirose, K. Nishita, H. Niimi, Influence of distribution of additives on electrical potential barrier at grain boundaries in ZnO-based multilayered chip varistor, J. Appl. Phys. 100 (8) (2006) 083706.1–083706.7.
[12] W.P. Chen, S.G. Lu, H.L.W. Chan, Influence of electroless nickel plating on *I–V* characteristics and its implications for reliability in ZnO-based ceramic varistors, Mater. Sci. Eng. B 99 (1–3) (2003) 70–73.
[13] M.A. Ramirez, W. Bassi, P.R. Bueno, E. Longo, J.A. Varela, Comparative degradation of ZnO- and SnO_2-based polycrystalline non-ohmic devices by current pulse stress, J. Phys. D: Appl. Phys. 41 (2008) 122002.1–122002.5.
[14] M.A. Ramirez, M. Cilense, P.R. Bueno, E. Longo, J.A. Varela, Comparison of non-ohmic accelerated ageing of the ZnO- and SnO_2-based voltage dependent resistors, J. Phys. D: Appl. Phys. 42 (2009), 015503.1-015503.4.
[15] T.Y. Li, Y. Wang, L. Dong, Novel Pr_6O_{11} varistor, J. Cent. South. Univ. Technol. 14 (S2) (2007) 42–46.
[16] Z.C. Kang, L. Eyring, Fluorite structural principles: disordered a-phase to ordered intermediate phases in praseodymia, J. Alloys Compd. 275–277 (1998) 721–724.
[17] C.M. Wang, J.F. Wang, C.L. Wang, H.C. Chen, W.B. Su, G.Z. Zang, P. Qi, Nonlinear electrical characteristics of SnO_2•CuO ceramics with different donors, J. Appl. Phys. 97 (12) (2005) 126103.1–126103.3.
[18] V.R. Kolbunov, A.I. Ivon, I.M. Chernenko, Influence of a high conductivity additive on the electrical properties of vanadium dioxide-based ceramics, J. Eur. Ceram. Soc. 23 (9) (2003) 1435–1439.
[19] E.R. Leite, J.A. Varela, E. Longo, A new interpretation for the degradation phenomenon of ZnO varistors, J. Mater. Sci. 27 (19) (1992) 5325–5329.
[20] L.M. Levinson, H.R. Philipp, High-frequency and high-current studies of metal oxide varistors, J. Appl. Phys. 47 (7) (1976) 3116–3121.
[21] A.A. Sagüés, S.C. Kranc, E.I. Moreno, Evaluation of electrochemical impedance with constant phase angle component from the galvanostatic step response of steel in concrete, Electro Elect. Chim. Acta 41 (7–8) (1996) 1239–1243.
[22] A.C. Caballero, D. Fernández Hevia, J. de Frutos, M. Peiteado, J.F. Fernández, Bulk grain resistivity of ZnO-based varistors, J. Electroceram. 13 (7–8) (2004) 759–763.
[23] Z.C. Kang, L. Eyring, Lattice oxygen transfer in fluorite-type oxides containing Ce, Pr, and/or Tb, J. Alloys Compd. 155 (1) (2000) 129–137.
[24] R.D. Shannon, Revised effective ionic radii and systematic studies of interatomie distances in halides and chaleogenides, Acta Crystallogr. A32 (1976) 751–767.